DC-Link Voltage Coordinated-Proportional Control for Cascaded Converter with Zero Steady-State Error and Reduced System Type

DC-Link Voltage Coordinated-Proportional Control for Cascaded Converter with Zero Steady-State Error and Reduced System Type

Yanjun Tian，*Student Member, IEEE,* Poh Chiang Loh, Fujin Deng, *Member, IEEE*, Zhe Chen, Senior Member, *IEEE.* Yanting Hu, *Senior Me*m*ber, IEEE*

Abstract—**Cascaded converter is formed by connecting two sub-converters together, sharing a common intermediate DC-link voltage. Regulation of this DC-link voltage is frequently realized with a Proportional-Integral (PI) controller, whose high gain at DC helps to force a zero steady-state tracking error. Such precise tracking is however at the expense of increasing the system type, caused by the extra pole at the origin introduced by the PI controller. The overall system may hence be tougher to control. To reduce the system type while preserving precise DC-link voltage tracking, this paper proposes a coordinated control scheme for the cascaded converter, which uses only a proportional DC-link voltage regulator. The resulting converter is thus dynamically faster, and when compared with the conventional PI-controlled converter, it is less affected by impedance interaction between its two sub-converters. The proposed scheme can be used with either unidirectional or bidirectional power flow, and has been verified by simulation and experimental results presented in the paper.**

Index Terms— **Cascaded Converter, Dual Active Bridge, Impedance Matching, Proportional Control, Coordinated Control**

I. INTRODUCTION

POWER electronic converters have widely been used with different electrical systems including photovoltaic (PV), energy storage, solid-state transformer, and many others [1-5]. Recently, the introduction of DC and AC active distribution networks and micro-grids [6-8] is also an area, where power converters will essentially be used for interconnection. Among the converters proposed, cascaded converters will probably be the most flexible since they are realized by connecting two or more sub-converters together. For the case of DC-AC

Yanjun Tian, Poh Chiang Loh, Fujin Deng, Zhe Chen, are with the Department of Energy Technology, Pontoppidanstraede 101, Aalborg 9220, Denmark, (phone: +45 2445 4635; e-mail: yti@et.aau.dk, pcl@et.aau.dk, fde@et.aau.dk ,zch@et.aau.dk).
Yanting Hu is with Faculty of Science and Engineering, University of Chester, Chester, CH2 4NU UK, e-mail: y.hu@chester.ac.uk
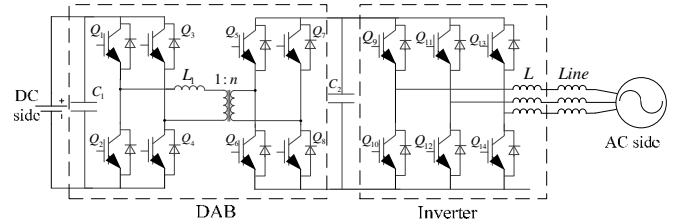
Fig. 1. Cascaded converter implemented with DAB converter and voltage-source inverter.

conversion, the sub-converters will usually be a DC-DC converter and a typical three-phase voltage-source inverter. Where galvanic isolation is required, the DC-DC converter must have a high-frequency transformer included, like the Dual-Active-Bridge (DAB) converter shown in Fig. 1, together with a voltage-source inverter. The DAB converter has previously been used as a solid-state transformer because of its attractive high power density, bidirectional power flow ability and zero voltage switching [9-11]. It is therefore the chosen sub-converter for cascading with the inverter shown in Fig. 1. Other sub-converters can also be cascaded without affecting findings uncovered in the paper.

Referring to Fig. 1, between the two sub-converters is a DC-link capacitor C_2 for smoothing voltage ripple in the steady state [12], which otherwise, may affect stability of the cascaded converter [13]. Reducing ripple by increasing C_2 alone is however not economically attractive. It is therefore conventional for the voltage V_{dc} across C_2 to be regulated by a controller of one of the sub-converters [14-19]. The other sub-converter will then control power flow through the overall cascaded converter.

For regulating V_{dc} with zero steady-state error, a Proportional-Integral (PI) controller is frequently used at the expense of increasing the system type [20]. To avoid that, this paper proposes a coordinated control scheme for the cascaded converter, which uses only a proportional controller for enforcing precise DC-link voltage tracking. The resulting converter with lower system type is easier to damp and stabilize, and has a more decoupled impedance interaction between its sub-converters at their common terminals. The proposed control is thus more effective than conventional PI control, as verified in simulation and experiment.

The obtained results and formulated concepts are organized into four sections after this introduction. Section II begins by discussing the modeling and conventional control of the considered cascaded converter. Section III continues with the modeling and analysis, but with the proposed coordinated-proportional scheme included for DC-link voltage regulation. Section IV then shows the obtained results, before concluding the paper in Section V.

II. CONVENTIONAL CONTROL

A. DAB Modeling and Control

Fig. 1 shows the DAB converter with two full-bridges and a high or medium frequency transformer for providing galvanic isolation. Switches of the full-bridges are also drawn with capacitors in parallel, which when sized appropriately, will resonate with the transformer leakage inductance L_1 needed for zero voltage switching [21]. Control wise, the two full-bridges are usually square-wave modulated with an appropriate phase-shift inserted between them for fast regulation of power flow [22]. Typical waveforms demonstrating such control are shown in Fig. 3, where two square waves phase-shifted by $\emptyset$ can clearly be seen.

Power flow P from the leading to lagging bridge can then be expressed as [19], [23]:

$$P = \frac{nV_1 V_2}{2\pi^2 f L_1}\phi(\pi - |\phi|) \tag{1}$$

where f is the square-wave switching frequency, and V_1 and V_2 are the input and output voltages of the DAB converter, respectively. Power P can therefore be controlled by varying $\emptyset$, which theoretically, will maximize when $\emptyset$ equals $\frac{\pi}{2}$. After which, P can only be increased by reducing f and / or L_1.
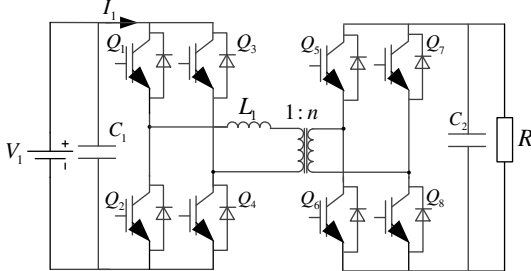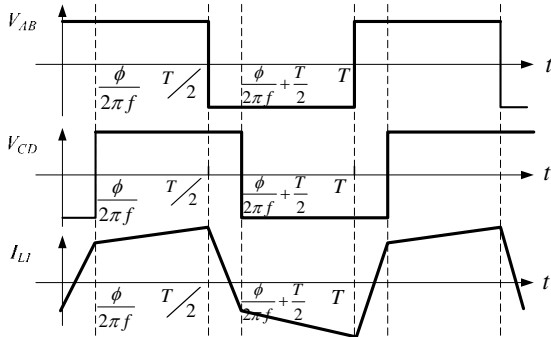

Fig. 2. Topology of DAB converter.

V_{AB} -Transformer primary side voltage I_{L1} -Transformer primary side current
V_{CD} -Transformer secondary side voltage I_1 -Primary side H-bridge input current

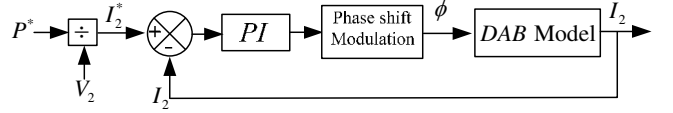Fig. 3. Operating waveforms of DAB converter ($V_1 < \frac{1}{n}V_2$, n -turns ratio).

Fig. 4. Power flow control diagram of DAB converter (DAB model substituted from (3)).

From (1), the output current I_2 of the DAB converter can be expressed as:

$$I_2 = \frac{nV_1}{2\pi^2 f L_1}\phi(\pi - |\phi|) \tag{2}$$

Current control of I_2 by varying $\emptyset$ is therefore viable, but nonlinear. Small-signal linearization can then be performed on (2) to obtain (3).

$$\hat{I}_2 = \frac{nV_1}{2\pi^2 f L_1}\phi(\pi - 2\phi)\hat{\phi} \tag{3}$$

where $\hat{\phi}$ and $\hat{I}_2$ are the small incremental phase shift and output current, respectively.

Incremental $\hat{\phi}$ is conventionally obtained from a PI controller after processing the current error as input. Open-loop transfer function of the current control loop $G_{I-DAB}(s)$ can thus be written as (4), while its closed function is given by (5).

$$G_{I-DAB}(s) = \frac{K_{P-DAB}s + K_{i-DAB}}{s}\frac{nV_1}{2\pi^2 f L_1}(\pi - 2\phi) \tag{4}$$

$$G_{DAB}(s) = \frac{G_{I-DAB}(s)}{1 + G_{I-DAB}(s)} \tag{5}$$

where K_{P-DAB} and K_{i-DAB} are the proportional and integral gains of the PI controller used for current (or power) regulation. Illustrative block diagram of the current control scheme is shown in Fig. 4, where current reference I_2^* is computed from the demanded power transfer P^* and output voltage V_2 of the DAB converter [21]. Power reference P^* is, in turn, produced by an outer loop, which can be a second PI controller for regulating the output voltage V_2 of the DAB converter. Similar double-loop structure has also recently been recommended for DAB converter used in solid-state transformers [24 -26].

Alternatively and much earlier than [24], a single DC-link voltage loop has been used for generating the desired phase shift needed by the DAB converter. Differences between the single- and double-loop structures are well-established in control theory, and hence not further discussed. In this paper, the double-loop structure is the conventional scheme chosen for comparison simply because it is the more recent existing scheme, which the proposed coordinated-proportional scheme aims to outperform.

B. Inverter Modeling and Control

Fig. 5 shows a voltage-source inverter connected to the grid through an inductive filter L with parasitic resistance r. Under power control, the inverter is usually modeled in the d-q frame after applying Park transformation to its parameters [27]. Its power output can then be computed using (6) and (7).

$$P = \frac{3}{2}\left(U_d I_d + U_q I_q\right) \tag{6}$$

$$Q = -\frac{3}{2}\left(U_d I_q - U_q I_d\right) \tag{7}$$

where U_d and U_q are the d-q output voltages, and I_d and I_q are
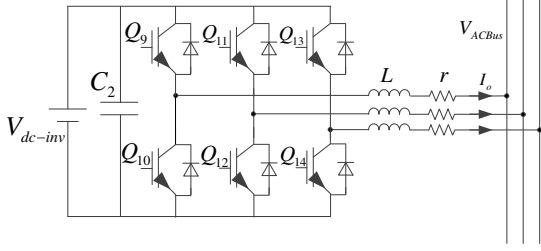

Fig. 5. Topology of grid-connected voltage-source inverter.
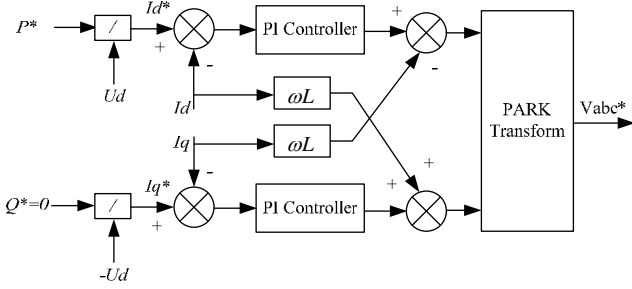

Fig. 6. Power flow control diagram of grid-connected inverter.

the d-q output currents. Further orienting the d-axis to be along the grid voltage vector leads to $U_q = 0$, which when substituted to (6) and (7), gives (8) and (9) for computing current references from the demanded power flow.

$$I_d^* = \frac{2}{3}\frac{P^*}{U_d} \tag{8}$$

$$I_q^* = -\frac{2}{3}\frac{Q^*}{U_d} \tag{9}$$

Equations (8) and (9) have been included in Fig. 6, which shows the conventional current control scheme for an inverter with PI controllers used for precise steady-state tracking [28, 29]. Also included in the figure are two cross ωL branches for decoupling the L-filter in the d-q frame. The d and q-axis control blocks can then be analyzed separately with their common open-loop transfer function $G_I(s)$ expressed as:

$$G_I(s) = \frac{V_{dc-inv}}{2}\frac{K_{P-INV}s + K_{i-INV}}{s}\frac{1}{Ls + r} \tag{10}$$

where V_{dc-inv} is the input DC voltage of the inverter in Fig. 5, and K_{P-INV} and K_{i-INV} are the proportional and integral gains of the PI controllers used in Fig. 6. Closed-loop transfer function $G_{INV}(s)$ of Fig. 6 can eventually be derived by substituting (10) to the following.

$$G_{INV}(s) = \frac{G_I(s)}{1 + G_I(s)} \tag{11}$$

C. Control of Cascaded Converter

Conventionally, a cascaded converter is controlled by designing one sub-converter to regulate its DC-link voltage and the other sub-converter to regulate its power flow [30]. Both sub-converters use PI controllers for eliminating steady-state errors. The PI transfer function is given in (12), which has earlier been notated with appropriate subscripts when deriving

open-loop transfer functions in (4) and (10) for the individual sub-converters.

$$G_{PI}(s) = \frac{K_P s + K_i}{s} \tag{12}$$

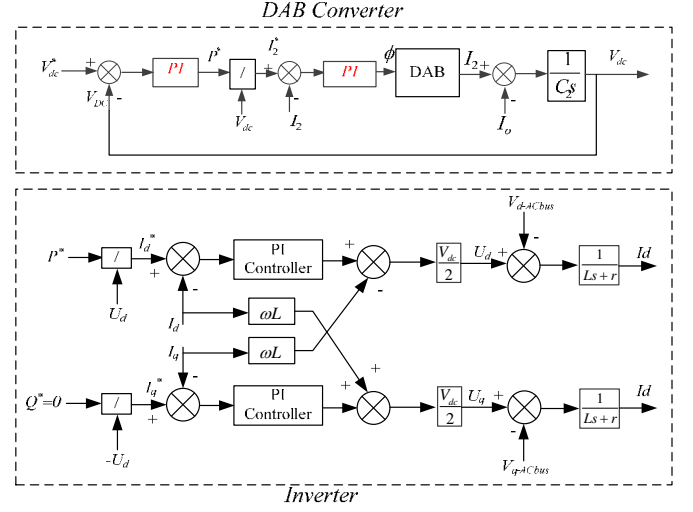For illustrating how the conventional control is organized,

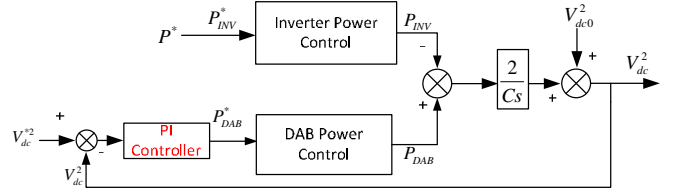Fig. 7. Conventional control scheme for cascaded converter.

Fig. 8. Energy-based conventional control block diagram for cascaded converter.

Fig. 7 shows the DAB converter regulating the common DC-link voltage, and the inverter regulating the overall power flow. PI controllers used with the DAB converter are therefore for removing the outer DC-link voltage error [21] and improving the inner current tracking performance [24]. On the other hand, PI controllers used with the inverter are for removing d-q current or power tracking errors.

Closed-loop transfer functions of Fig. 7 can subsequently be derived, but would simply involve finding the function related to the outer DC-link voltage loop only. This is because other functions describing the inner DAB current loop and inverter single current loop have already been found in (5) and (11). The function related to the outer DC-link voltage loop is however non-trivial to derive because of the nonlinearity between DC-link voltage and output power of the DAB converter. Such nonlinearity can usually be avoided by considering the linear energy model of the cascaded converter like shown in Fig. 8.

In the figure, P_{INV}^* and P_{DAB}^* are power references for the inverter and DAB converter, respectively. Reference P_{DAB}^* is obtained from a PI controller, after processing the error between reference and measured squared DC-link voltages, notated respectively as V_{dc}^{*2} and V_{dc}^2. The power references, when multiplied with their respective inverter and DAB models, then give the actual powers P_{INV} and P_{DAB} flowing through the two sub-converters. Their subtraction ($P_{DAB} - P_{INV}$), scaled

integration $2/(Cs)$, and addition to nominal value V_{dc0}^2 finally give the squared DC-link voltage for feedback. The difference here is thus the feeding back of V_{dc}^2 for linearization purpose, rather than V_{dc}. Such linearization will not significantly change the small-signal dynamic, because of (13) which proves that the squared and non-squared DC-link voltage errors are approximately equal, after scaled by $2V_{dc}^*$.

$$V_{dc}^{*2} - \left(V_{dc}^* + \Delta V_{dc} \right)^2 \approx \left[V_{dc}^* - \left(V_{dc}^* + \Delta V_{dc} \right) \right] \Delta 2 V_{dc}^* \qquad (13)$$

where ΔV_{dc} is the small perturbed DC-link voltage.

Fig. 8 is thus appropriate for evaluating the DC-link voltage dynamic, from which, the following open-loop transfer function $G_{V_{dc}^2}(s)$ can be derived.

$$G_{V_{dc}^2}(s) = \frac{K_P s + K_i}{s} G_{DAB}(s) \frac{2}{Cs} \qquad (14)$$

where $G_{DAB}(s)$ is the inner power control transfer function of the DAB converter obtained from (5). According to classical control theory [31], the system type of (14) is thus raised by one because of the additional pole at the origin introduced by the PI controller. System type can be defined based on the following open-loop transfer function $G(s)$ of a unity-feedback control system.

$$G(s) = \frac{K \prod_{j=1}^{m} \left(\tau_j s + 1 \right)}{s^N \prod_{i=1}^{n} (T_i s + 1)} \qquad (15)$$

In the dominator, s^N indicates the number of poles at the origin or the number of integrations associated with the open-loop transfer function. This number N is defined as the system type. As N increases, accuracy improves, but may aggravate the stability problem. Therefore, although (14) works in general, it may be challenging to formulate an alternative control scheme that will not raise the system type, while not compromising the desired voltage tracking. For that, this paper proposes a coordinated control scheme using only a proportional controller for regulating the DC-link voltage. Precise voltage tracking is still retained by designing the scheme to incorporate the principle of balanced power flow at the DC-link of any cascaded converter. More details are provided in the following section.

III. COORDINATED-PROPORTIONAL CONTROL

A. *Operating Principles*

Coordinated-proportional control of the cascaded converter employs both the DAB converter and inverter for regulating the DC-link voltage. It is therefore different from the conventional control discussed in Section II, where only the DAB converter regulates the DC-link by transferring more power to it when its voltage drops, and vice versa. Involving the inverter for DC-link regulation would however require the control action to be reversed since the inverter raises the DC-link voltage by drawing lesser power from it. The difference in power between the DAB converter and inverter will then be integrated by the DC-link capacitor to give a total voltage increment.

Such coordinated DC-link voltage control is shown in Fig. 9, which when compared with Fig. 7, is noted to use the same inner power loops. The main difference is the DC-link voltage control in Fig. 9, which uses a simple proportional controller rather than the usual PI controller. The controller output is also fed to both power loops of the DAB converter and inverter, rather than to the DAB converter alone in Fig. 7. It should however be noted that the controller output to the inverter is negated, unlike that to the DAB converter. In other words, power references for the DAB converter and inverter are $P_{DAB}^* = P^* + \Delta P$ and $P_{INV}^* = P^* - \Delta P$, respectively, where ΔP is the proportional controller output and P^* is the common steady-state power reference shared by both sub-converters.

In general, feeding ΔP to both sub-converters has the advantage of improving ride-through when one of the sub-converters fails. For example, in case of DAB converter failure, the inverter will still regulate the DC-link voltage with the proposed scheme, but not the conventional scheme which relies solely on the DAB converter for DC-link voltage regulation. The only compromise experienced by the proposed scheme during the fault period is a non-zero DC-link voltage
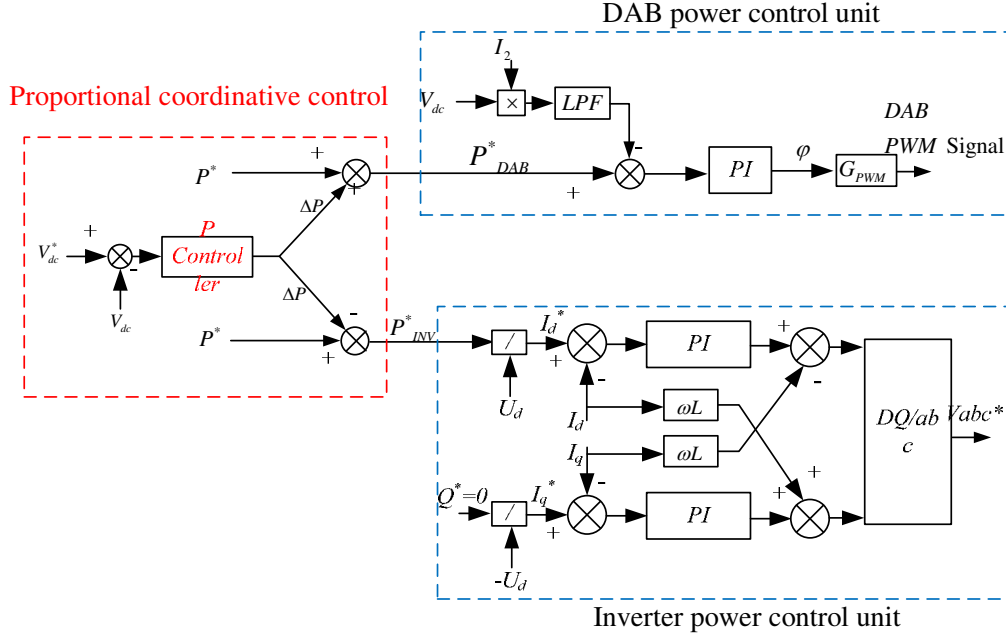
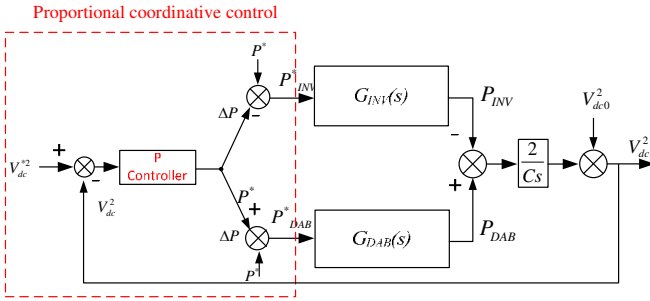Fig. 9. Coordinated-proportional control scheme for cascaded converter.

Fig. 10. Energy-based coordinated-proportional control block diagram for cascaded converter.

error because of the proportional voltage controller used. This error will however not exist during normal operating conditions, as explained below.

Returning to Fig. 9 and expressing it in its linearized energy model gives rise to Fig. 10 for studying the DC-link voltage control in terms of V_{dc}^2. Assuming now a small DC-link voltage error of ΔV_{dc} is unintentionally inserted, the DC-link voltage becomes:

$$V_{dc} = V_{dc}^* + \Delta V_{dc} \qquad (16)$$

The incremental power ΔP, and power references P_{INV}^* and P_{DAB}^* to the inverter and DAB converter can then be expressed as:

$$\Delta P = K_P \Delta V_{dc} \qquad (17)$$

$$P_{INV}^* = P^* - \Delta P \qquad (18)$$

$$P_{DAB}^* = P^* + \Delta P \qquad (19)$$

A power difference thus exists between the DAB converter and inverter, which when integrated by the DC-link capacitor, gives the following squared voltage variation.

$$\Delta V_{dc}^2 = 4 \frac{1}{Cs} \Delta P \qquad (20)$$

In the steady state, ΔP must be zero since the cascaded converter transfers and not consumes power. In other words, power through the DAB converter must fully be delivered by the inverter to the load. From (20), ΔV_{dc}^2 and hence ΔV_{dc} must then be zero even though only a simple proportional voltage controller with gain K_P is used. With the proportional controller, open-loop transfer function of the DC-link voltage control in Fig. 10 can also be expressed as:

$$G_{V_{dc}^2}(s) = K_P \left[G_{DAB}(s) + G_{INV}(s) \right] \frac{2}{Cs} \qquad (21)$$

where $G_{DAB}(s)$ and $G_{INV}(s)$ are from (5) and (11), respectively.

Bode diagrams of (14) for the conventional scheme and (21) for the proposed scheme can subsequently be plotted in Fig. 11 for comparison using parameters listed in the Appendix. As seen from Fig. 11(a), phase-shift introduced by the conventional scheme at low frequency is $-180°$, while that introduced by the proposed scheme in Fig. 11(b) is $270°$ or $-90°$. DC-link voltage controlled by the proposed scheme thus resembles a typical first-order system, while the conventional approach leads to a second-order system. This reduction of system order by the proposed scheme is implicitly related to its
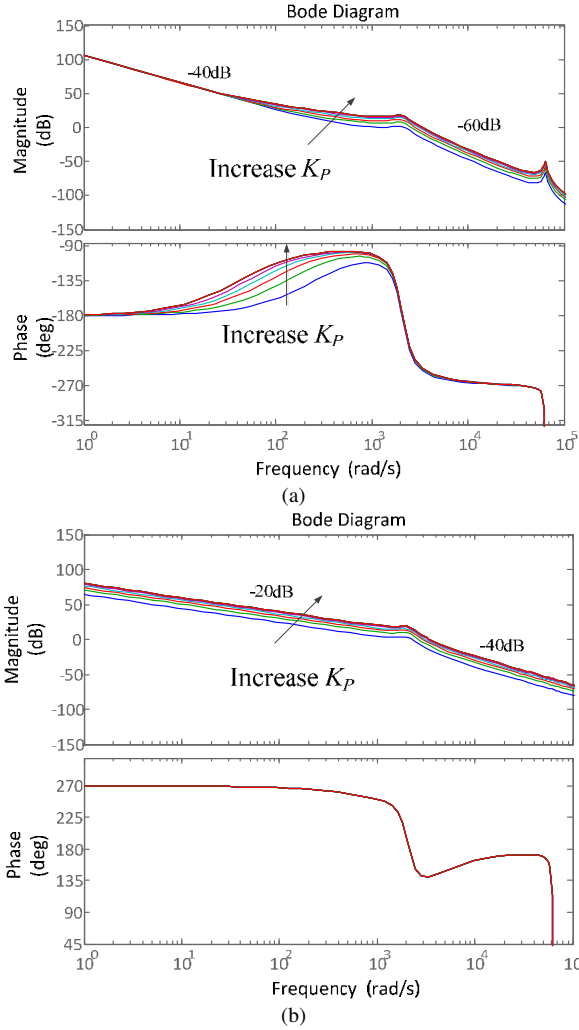
Fig. 11. Open-loop Bode diagrams plotted with (a) conventional and (b) proposed DC-link voltage control

Fig. 12. Energy-based block diagrams for (a) conventional and (b) proposed schemes with P^* as input and V_{dc}^2 as output.

reduction of system type by one because of the absence of an extra pole at the origin introduced by the integral term of a PI controller.

B. DC-Link Voltage Oscillation Perturbed by Power Reference Variation

Referring to Fig. 8 and Fig. 10, besides the DC-link voltage command V_{dc}^*, the measured DC-link voltage V_{dc} of the cascaded converter will be influenced by the common power reference P^*. To study their relationship, Fig. 8 and Fig. 10 are redrawn in Fig. 12(a) and (b) with P^* placed on the left as input and V_{dc}^2 placed on the right as output [19]. Bode diagrams showing how interference from P^* affects oscillation of V_{dc}^2 can then be plotted, as shown in Fig. 13. The general observation noted is a higher attenuation, and hence a smaller V_{dc}^2 oscillation created by the proposed scheme when P^* is perturbed. The proposed scheme is thus more capable of maintaining a stable DC-link voltage under perturbed conditions.
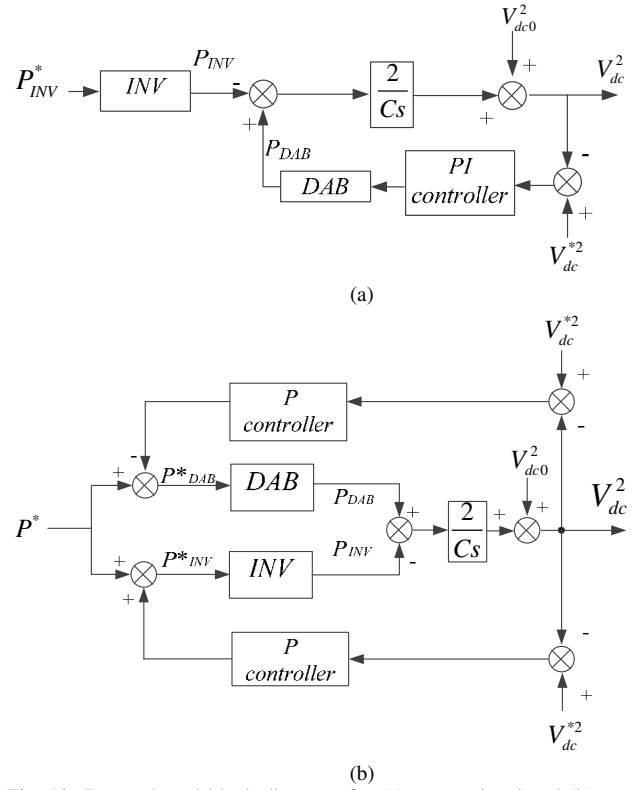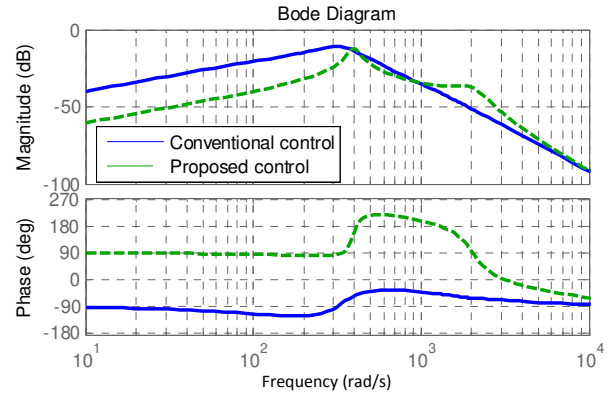

Fig. 13. Bode diagrams plotted for Fig. 12(a) and (b).

C. Impedance Interaction between Sub-Converters

A feature unique to the cascaded converter is its internal impedance interaction between its two sub-converters. More specifically, the output impedance of the DAB converter will interact with the input impedance of the inverter, if power is sent from the DAB converter to the inverter. Such interaction may cause system instability [32, 33], and is commonly expressed as T in (22).

$$T = \frac{Z_o}{Z_{in}} \qquad (22)$$

where Z_o is the output impedance of the sending DAB converter, and Z_{in} is the input impedance of the receiving inverter. Both impedances can be computed from small-signal modeling, and are respectively expressed as:

$$Z_o = -\frac{\hat{V}_{DAB}}{\hat{I}_{DAB}} \quad I_2 = \frac{nV_I}{2\pi^2 fL_I}\phi\left(\pi - |\phi|\right) \tag{23}$$

$$Z_{in} = \frac{\hat{V}_{inv}}{\hat{I}_{inv}} \quad I_2 = \frac{nV_I}{2\pi^2 fL_I}\phi\left(\pi - |\phi|\right) \tag{24}$$

where $\hat{V}_{DAB}$ and $\hat{I}_{DAB}$ are the small-signal output voltage and current of the DAB converter, and $\hat{V}_{inv}$ and $\hat{I}_{inv}$ are the small-signal input voltage and current of the inverter. These variables are extracted from the intermediate DC-link of the cascaded converter, which means $\hat{V}_{DAB}$ and $\hat{V}_{inv}$ are equal since they represent the same small-signal perturbed DC-link voltage $\hat{V}_{dc}$.

With conventional control, the DAB converter solely regulates the DC-link voltage, while the inverter solely regulates the power flow of the cascaded converter. Its small-signal output current from the DAB converter and input current to the inverter can thus be expressed as:

$$\hat{I}_{DAB} = \frac{\hat{P}_{DAB}}{V_{dc} + \hat{V}_{dc}} = -\frac{\hat{V}_{dc}G_{PI}(s)G_{DAB}(s)}{V_{dc} + \hat{V}_{dc}} \tag{25}$$

$$\hat{I}_{inv} = \left(\frac{P^*}{V_{dc} + \hat{V}_{dc}} - \frac{P^*}{V_{dc}}\right)G_{inv}(s) = -\frac{\hat{V}_{dc}P^*}{V_{dc}(V_{dc} + \hat{V}_{dc})}G_{inv}(s) \tag{26}$$

where $G_{PI}(s)$ is the PI transfer function from (12), $G_{DAB}(s)$ is the DAB transfer function from (5), and $G_{inv}(s)$ is the inverter transfer function from (11). The DAB output impedance and inverter input impedance under conventional control can thus be computed as:

$$Z_o = \frac{V_{dc} + \hat{V}_{dc}}{G_{PI}(s)G_{DAB}(s)} \tag{27}$$

$$Z_{in} = -\frac{V_{dc}(V_{dc} + \hat{V}_{dc})}{P^*G_{inv}(s)} \tag{28}$$

where $Z_{in} = -\frac{V_{dc}(V_{dc} + \hat{V}_{dc})}{P^*G_{inv}(s)}$ (28) will be negative at low frequency under constant power control [34, 35]. Impedance interaction T from (22) under conventional control can then be expressed as (29), which simply, is a negative high-pass function multiplied with $G_{inv}(s)/G_{DAB}(s)$. The negative high-pass function introduces an additional $-90°$ phase-shift to T, and causes its gain to vary with P^* (K_p and K_i are constant, while V_{dc} is usually approximately constant).

$$T = \frac{-P^*s}{V_{dc}(K_p s + K_i)}\frac{G_{inv}(s)}{G_{DAB}(s)} \tag{29}$$

Now, with the proposed coordinated-proportional control scheme, small-signal output current of the DAB converter and input current of the inverter can be expressed as:

$$\hat{I}_{DAB} = \frac{\hat{P}_{DAB}}{V_{dc} + \hat{V}_{dc}} = -\frac{\hat{V}_{dc}K_P G_{DAB}(s)}{V_{dc} + \hat{V}_{dc}} \tag{30}$$

$$\hat{I}_{inv} = \left(\frac{P^* + \hat{P}^*}{V_{dc} + \hat{V}_{dc}} - \frac{P^*}{V_{dc}}\right)G_{inv}(s) = \frac{\hat{V}_{dc}V_{dc}K_P - \hat{V}_{dc}P^*}{V_{dc}(V_{dc} + \hat{V}_{dc})}G_{inv}(s) \tag{31}$$

Output impedance of the DAB converter and input impedance of the inverter can then be expressed as:

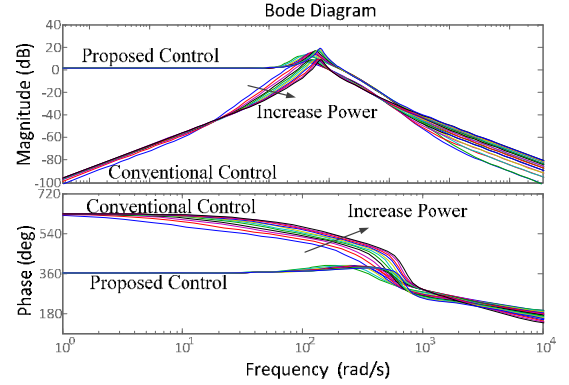$$Z_o = \frac{V_{dc} + \hat{V}_{dc}}{K_{VP}G_{DAB}(s)} \tag{32}$$

Fig. 14. Bode diagrams showing impedance interaction within cascaded converter when load changes from 1 to 10 kW.

$$Z_{in} = \frac{V_{dc}(V_{dc} + \hat{V}_{dc})}{(K_{VP}V_{dc} - P^*)G_{inv}(s)} \quad Z_{in} = \frac{V_{dc}(V_{dc} + \hat{V}_{dc})}{(K_{VP}V_{dc} - P^*)G_{inv}(s)} \tag{33}$$

Impedance interaction T with the proposed control can eventually be determined as:

$$T_m = k\frac{G_{inv}(s)}{G_{DAB}(s)} \tag{34}$$

$$k = \frac{(K_P V_{dc} - P^*)}{V_{dc}K_P} \tag{35}$$

where k is a simple gain, which again varies with P^*. No phase shift is however added to $G_{inv}(s)/G_{DAB}(s)$, unlike the conventional scheme.

To better illustrate how (29) and (34) differ, their Bode diagrams are plotted in Fig. 14 using the same parameters listed in the appendix for both control schemes. As seen, the 20 dB/dec increasing slope and $-90°$ ($= 630°$ in the figure) phase-shift at low frequency are characteristics introduced by the negative high-pass function of the conventional scheme. Such features are not seen with the proposed scheme, whose magnitude remains constant at zero phase. Impedance interaction introduced by the proposed scheme is thus purely resistive with no phase-shift problem over the full controllable range at low frequency. More importantly, variation of load or P^* in Fig. 14 will not change the characteristics of the proposed scheme greatly. It is thus less load-dependent. The conventional scheme, on the other hand, has varying characteristics as load changes. It is thus tougher to stabilize with constant control parameters, especially when the load changes greatly.

D. Design of Proportional Gain for DC-Link Voltage Control

Tuning of proportional gain used with the proposed control can be performed by referring to Fig. 15(a), where the common power reference P^*, viewed as a disturbance, has been ignored. Both DAB converter and inverter in the figure then form the plant transfer function, which when substituted from (5) and (11), gives Fig. 15(b) for showing how the DC-link voltage control varies with K_P. Clearly, increasing K_P does not change the phase, but will cause the magnitude curve to rise. Bandwidth of the DC-link voltage control is thus widened as K_P increases.

Fig. 16 next plots impedance interaction T of the proposed scheme when K_P varies. Also included in the figure are two
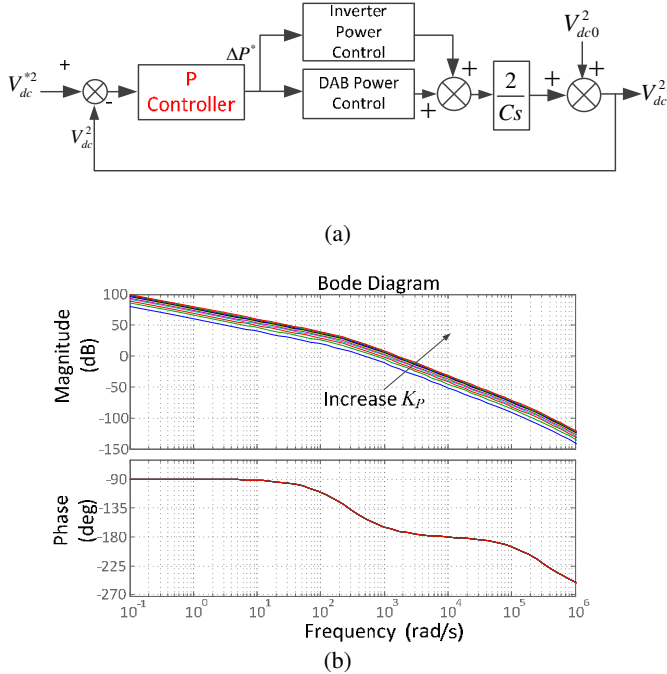

(a)

(b)

Fig. 15. Illustration of proposed DC-link voltage control (a) block diagram and (b) Bode diagram with increasing K_P.
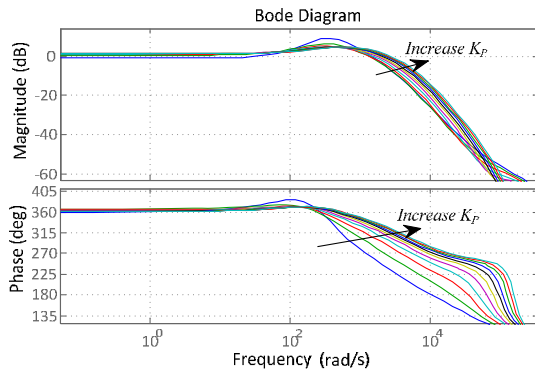

Fig. 16. Impedance interaction of proposed scheme with the variation of K_P

dashed lines for representing the ideal case with no impedance interaction. These dashed lines are clearly approached by characteristics of the proposed scheme as K_P increases. It is therefore advisable to maximize K_P so long as it remains in its stability zone.

E. DC-Link Voltage Damping

Damping response of the DC-link voltage can be analyzed by studying root loci of the conventional and proposed schemes, whose block diagrams are shown in Fig. 8 and Fig. 10, respectively. To not overcomplicate the root loci, smaller time constants of the inner DAB and inverter power control loops are ignored. The resulting loci obtained are shown in Fig. 17 for the conventional scheme and Fig. 18 for the proposed scheme. Each figure has its loci grouped into two different parts with part 1 of Fig. 17 noted to be nearer the vertical axis than that of Fig. 18. Part 1 of Fig. 18 or the proposed control scheme is thus damped more effectively. Part 2 of the proposed scheme is, on the other hand, placed on the real axis in the left half plane. It is therefore not oscillatory, as compared to part 2 of the

conventional scheme. Summarizing, damping performance of the proposed control is generally better than that of the conventional scheme.
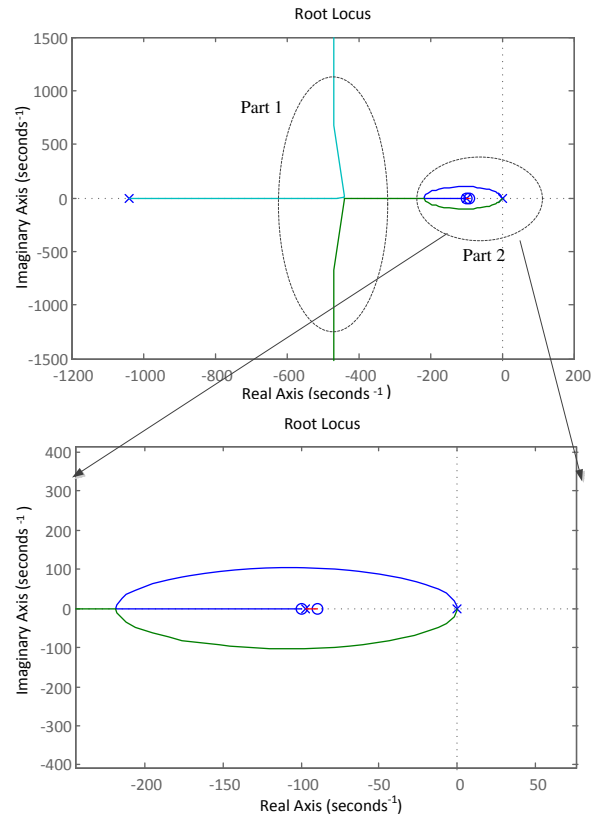

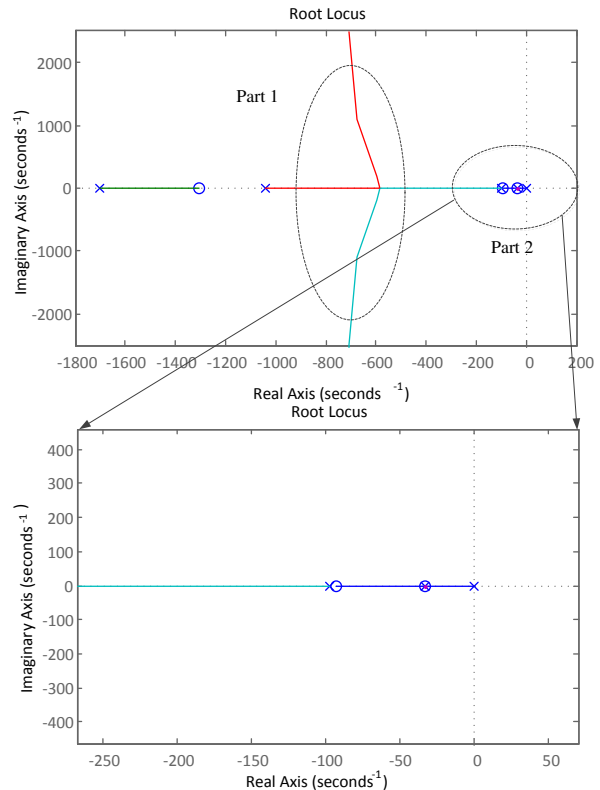Fig. 17. Root loci obtained with conventional DC-link voltage control.

Fig. 18. Root loci obtained with proposed DC-link voltage control.

IV. SIMULATION AND EXPERIMENT RESULTS

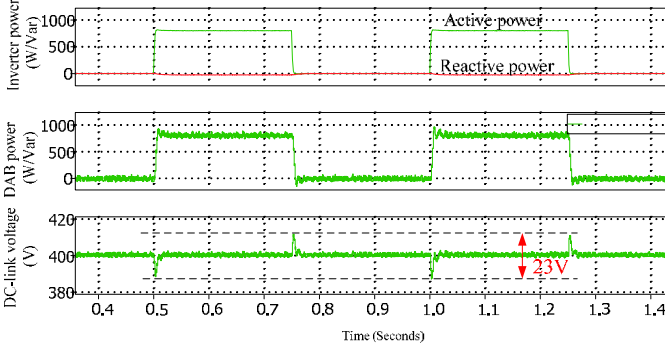For verification, simulations and experiments are performed

Fig. 19. Simulated (top to bottom) inverter powers, DAB power and DC-link voltage with conventional control and P^* stepping.
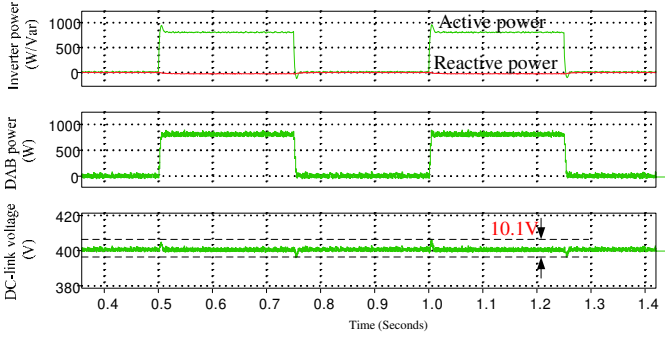

Fig. 20. Simulated (top to bottom) inverter powers, DAB power and DC-link voltage with proposed control and P^* stepping.

with the same proportional DC voltage control gain used for both control schemes. The conventional scheme has an additional integral gain, whose value and those of other system parameters are given in the appendix. The same power controllers for DAB converter and inverter are also used for both control schemes.

A. Simulation Results

The cascaded converter in Fig. 1 is simulated using the *PLECS* software. For the first simulation, power reference P^* is step-changed between 0 W and 800 W with a period of 0.5 s. Corresponding results produced are shown in Fig. 19 and Fig. 20. Fig. 19, in particular, shows a 23-V peak-to-peak DC-link voltage oscillation produced by the conventional scheme. This voltage oscillation is reduced to 10.1 V peak-to-peak by the proposed scheme in Fig. 20. Effectiveness of the proposed scheme in terms of blocking interference from P^* is thus demonstrated.

The second simulation is performed with the DC-link voltage reference V_{dc}^* step-changed between 362.5 V and 337.5 V with a period of 0.5 s. Fig. 21 shows the measured DC-link voltage with typical second-order overshoot and oscillation observed when the conventional scheme is used. Such features are however not seen in Fig. 22 with the proposed scheme, which as proven earlier, is a dynamically faster first-order system. Sharing of DC-link voltage regulation between the sub-converters ensured by the proposed scheme has also led to a smaller power variation experienced by the DAB converter in Fig. 22. The same power variation is however imposed on the

inverter, which when controlled by the conventional scheme, will not experience any power variation like shown in Fig. 21. However, with the conventional scheme, the DAB converter
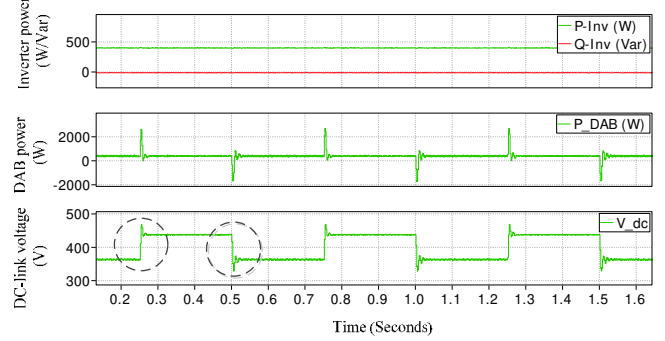

Fig. 21. Simulated (top to bottom) inverter powers, DAB power and DC-link voltage with conventional control and V_{dc}^* stepping.
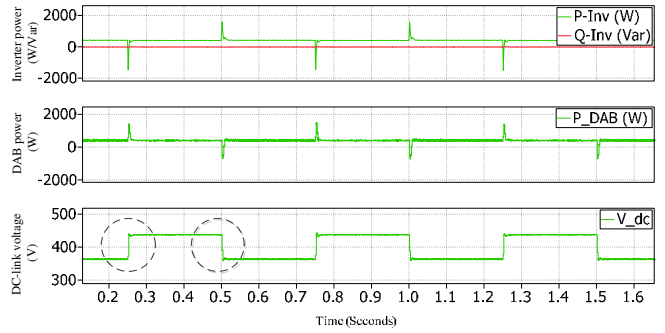

Fig. 22. Simulated (top to bottom) inverter powers, DAB power and DC-link voltage with proposed control and V_{dc}^* stepping.

carries a more than 4-kW peak-to-peak oscillation, which should generally be discouraged. The proposed scheme is thus preferred in terms of spreading stresses between the sub-converters.

B. Experimental Results

A scaled down prototype of the cascaded converter in Fig. 1 has been built using the same parameters as in simulations. The sub-converters are tested individually first with Fig. 23 showing the experiment waveforms measured from the transformer of the DAB converter. As expected, the primary voltage is 150 V, and the secondary voltage is 400 V, both switching at 10 kHz. The power transferred is 1 kW, which on the primary side, corresponds to a peak current of 19 A. Fig. 24 next shows the experimental output currents of the inverter during a 1.5-kW step transition from no load. Both sub-converters are obviously operating well, and are therefore cascaded to obtain results from Fig. 25 onwards.
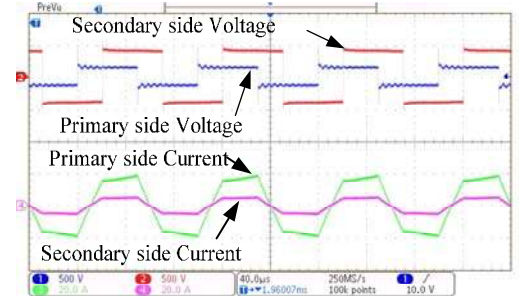
Fig. 23. Experimental waveforms measured from transformer of DAB converter.
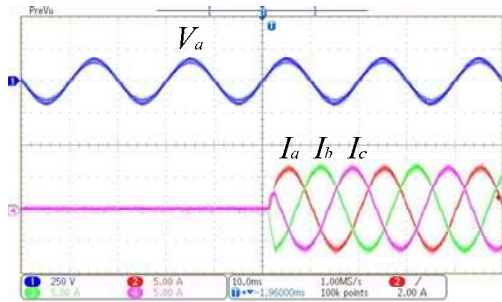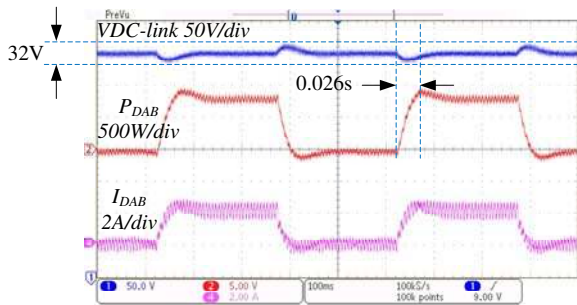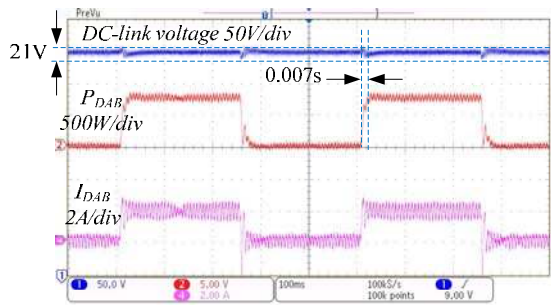

Fig. 24. Experimental AC waveforms measured from output of inverter.

(a)Conventional control
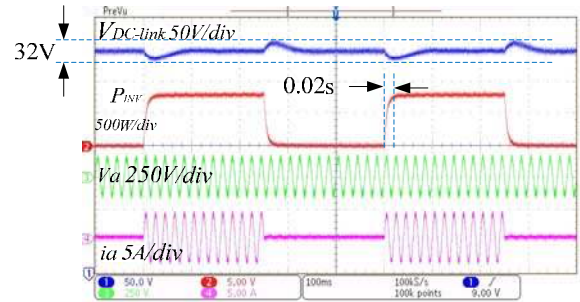

(b)Proportional control

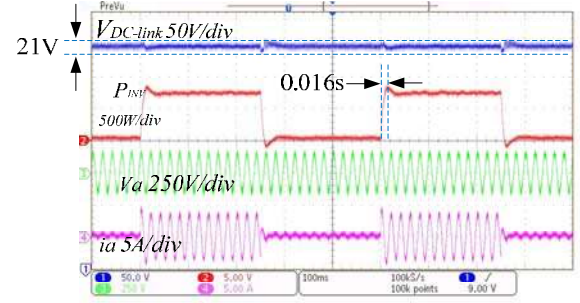Fig. 25. Experimental DC-link voltage, DAB power and output current under P^* stepping.

order control characteristics. Fig. 27(b) also

(a)Conventional control

(b)Proportional control

Fig. 26. Experimental DC-link voltage, inbverter power and output current under P^* stepping.

Proportional Control | *Conventional Control*

(a)DC-link voltage, DAB power and output current

Proportional Control | *Conventional Control*

DC-link voltage, inverter power and output current

Fig. 27. Transition from proposed to conventional scheme with V_{dc}^* stepping.

Fig. 25 shows the DC-link voltage $V_{DC-link}$, output power P_{DAB} and current I_{DAB} of the DAB converter when the power reference P^* changes between 0 and 800 W with a period of 0.5 s. As anticipated, conventional control leads to a larger peak-to-peak voltage oscillation of 32 V with a rising time of 0.026 s. Both oscillation and rising time are promptly reduced by the proposed scheme to 21 V and 0.007 s, which certainly, demonstrate the effectiveness of the proposed scheme. Fig. 26 next shows the DC-link voltage $V_{DC-link}$, output voltage V_a and current i_a of one phase of the inverter. Again, the rising time of the proposed scheme is smaller at 0.016 s, as compared to 0.02 s produced by the conventional scheme.

A second set of experiments is then performed with the DC-link voltage reference V_{dc}^* stepped between 362.5 V and 437.5 V with a period of 0.5 s. Fig. 27(a) and (b) show the waveforms obtained when changing from the proposed to conventional scheme. Both figures distinctly show that with the proposed scheme, the DC-link voltage recovers faster because of its first-

shows the disturbed inverter power and current when the proposed scheme is used, which certainly, are expected since the inverter shares the DC-link voltage regulation with the DAB converter. Features of the
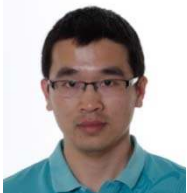
proposed scheme are therefore verified successfully by the presented experimental results.

V. CONCLUSION

In this paper, a coordinated-proportional control scheme for cascaded converter has been proposed. Unlike the conventional scheme, only a proportional controller is needed for DC-link voltage regulation without incurring significant steady-state error. The overall system type is thus reduced by one with faster dynamic, lesser load interference and smaller impedance interaction demonstrated. Moreover, by sharing responsibility, the proposed scheme helps to spread oscillatory stresses between the sub-converters, hence avoiding the single point of failure associated with the conventional scheme. Simulation and experimental results presented have verified these performance features, and hence the proposed coordinated-proportional control scheme.

VI. ACKNOWLEDGEMENT

VII. APPENDIX

TALBE1 PARAMETERS USED FOR ANALYSES, SIMULATION AND EXPERIMENTS

Parameter	Value
DAB power loop, K_{P-DAB}	0.0001
DAB power loop, K_{i-DAB}	0.0105
DAB switching frequency	10 kHz
DAB control bandwidth	1884 rad/s
Inverter current loop, K_{P-INV}	20
Inverter current loop, K_{i-INV}	500
Inverter switching frequency	10 kHz
Inverter control bandwidth	1570 rad/s
DC-link voltage controller, K_P	40
DC-link voltage controller, K_i	1000
Input voltage to cascaded converter, V_1	150 V
DC-link voltage, V_{dc}	400 V
AC output voltage of cascaded converter, V_{ACbus}	155 V
Transformer inductance, L_1	0.3 mH
AC filter inductance, L	6 mH
Capacitances, C_1 and C_2	300 μF each

Yanjun Tian (S'14) received the B.Sc. and M.Sc. degree in electrical engineering from the Yanshan University, Qinhuangdao, China in 2009 and 2012, respectively. He is currently working toward the PhD degree in the department of Energy Technology, Aalborg University Denmark.

His research interest includes distributed generation; and active distribution network control, focusing on the impedance interaction control, cascaded interface converter control and the parallel connected converter control.

Poh Chiang Loh received his B.Eng (Hons) and M.Eng from the National University of Singapore in 1998 and 2000 respectively, and his Ph.D from Monash University, Australia, in 2002, all in electrical engineering. He is a full Professor with the Department of Energy Technology, Aalborg University, Denmark. His interests are in power converters and their grid applications.

Fujin Deng (S'10, M'13) received the B.Eng. degree in electrical engineering from China University of Mining and Technology, Jiangsu, China, in 2005, the M.Sc. Degree in electrical engineering from Shanghai Jiao Tong University, Shanghai, China, in 2008, and the Ph.D. degree in energy technology from the Department of Energy Technology, Aalborg University, Aalborg, Denmark, in 2012.Currently, he is a Postdoctoral Researcher in the Department of Energy Technology, Aalborg University, Aalborg, Denmark.

His main research interests include wind power generation, multilevel converters, DC grid, high-voltage direct-current (HVDC) technology, and offshore wind farm-power systems dynamics.

Zhe Chen (M'95–SM'98) received the B.Eng. and M.Sc. degrees from Northeast China Institute of Electric Power Engineering, Jilin City, China, and the Ph.D. degree from University of Durham, U.K. He is a full Professor with the Department of Energy Technology, Aalborg University, Denmark. He is the leader of Wind Power System Research program at the Department of Energy Technology, Aalborg University and the Danish Principle Investigator for *Wind Energy* of *Sino-Danish Centre for Education and Research*.His research areas are power systems, power electronics and electric machines; and his main current research interests are wind energy and modern power systems. He has led many research projects and has more than 400 publications in his technical field.

Dr Chen is an Editor of the IEEE Transactions on Power Systems, an Associate Editor of the IEEE Transactions on Power Electronics, a Fellow of the Institution of Engineering and Technology (London, U.K.), and a Chartered Engineer in the U.K.

Yanting Hu (M'01, SM'08) received the B.Eng. and M.Sc. degrees from Northeast China Institute of Electric Power Engineering, China, and Ph.D. degree from De Montfort University, U.K.

Dr. Hu was with Department of Engineering and Physics Science, Glyndwr University, UK. From 2014, she works in the Faculty of Science and Engineering, University of Chester, UK

REFERENCES

[1] S. B. Kjaer, J. K. Pedersen, F. Blaabjerg, "A review of single-phase Grid-Connected Inverters for Photovoltaic Modules", *IEEE Transactions on Industry Application*, Vol. 41, NO. 5, September/Octorber 2005.

[2] S. Inoue, H. Akagi, "A Bidirectional DC–DC Converter for an Energy Storage System With Galvanic Isolation", *IEEE Transactions on Power Electronics*, Vol.22, NO.6, November 2007.

[3] J. M. Carrasco, L. G. Franquelo, J. T. Bialasiewicz, E. Galván, R. C. Portillo Guisado, M. Á. M. Prats, J. I. L., N. Moreno-Alfonso, "Power-Electronic Systems for the Grid Integration of Renewable Energy Sources: A Survey", *IEEE Transactions on Industrial Electronics*, Vol.53, NO.4, August, 2006.

[4] H. Qin, J. W.Kimball, "Solid-State Transformer Architecture Using AC-AC Dual-Active-Bridge Converter", *IEEE Transactions on Industrial Electronics*, Vol.60, NO.9, September 2013.

[5] D. G. Shah, M. L. Crow, "Stability Design Criteria for Dustribution System With Solid-State Transformers", *IEEE Transactions on Power Delivery*, Early Access.

[6] R. Lasseter:, "Mircrogrids," in *Proc. IEEE Power Eng. Soc. Winter Meet*, 2002, pp. 305-308.

[7] J. M. Guerrero, J. Matas, L. G. d. Vicuna, M. Castilla, J. Miret. "Decentralized Control for Parallel Operation of Distributed Generation Inverter Using Resistive Output Impedance." *IEEE Transactions on Industrial electronics*, Vol.54, NO.2April, 2007.

[8] P. C. Loh, and D. Li, Y. K. Chai, and F. Blaabjerg, "Hybrid AC-DC Microgrids With Energy Storages and Progressive Energy Flow Tuning ," *IEEE Trans. Power Electronics*, Vol. 28, NO. 4,pp. 1533-1542, Apr.2013.

[9] H. Bai, C. Mi, "Eliminate Reactive Power and Increase System Efficiency of Isolated Bidirectional Dual-Active-Bridge DC–DC Converters Using Novel Dual-Phase-Shift Control," *IEEE Transactions on Power Electronics*, Vol. 23, NO. 6, November 2008

[10] F. Krisme, J. W. Kolar, "Efficiency-Optimized High-Current Dual Active Bridge Converter for Automotive Applications," *IEEE Transactions on Power Electronics*, Vol. 59, NO. 7, July 2012.

[11] D. Segaran, D. G. Holmes, B. Peter McGrath, "Enhanced Load Step Response for a Bidirectional DC–DC Converter," *IEEE Transactions on Power Electronics*, Vol. 28, NO. 1, January 2013

[12] X. Zhang, C. Zhang, "PWM rectifier and control," *Machinery Industry Press*, October, 2003, pp.148-153.

[13] X. Zhang, X. Ruan, H. Kim, C. K. Tse, "Adaptive Active Capacitor Converter for Improving Stability of Cascaded DC Power Supply System ," *IEEE Transactions on Power Electronics*, Vol. 28, No. 4, April 2013.

[14] Z. Chen, W. Gao, J. Hu, X. Ye, "Closed-Loop Analysis and Cascade Control of a Nonminimum Phase Boost Converter," IEEE Transactions on Power Electronics, Vol. 26, NO. 4, April 2011.

[15] H. M. Hasanien, S. M. Muyeen, "Design Optimization of Controller Parameters Used in Variable Speed Wind Energy Conversion System by Genetic Algorithms," IEEE Transactions on Sustainable Energy, Vol. 3, NO. 2, April 2012.

[16] C. Y. Chan, " Investigation of voltage-mode controller for cascade boost converter," *IET Power Electron*, 2014, Vol. 7, Iss. 8, pp. 2060–2068.

[17] A. M. Rahimi, A. Emadi, "Active Damping in DC/DC Power Electronic Converters: A Novel Method to Overcome the Problems of Constant Power Loads", *IEEE Transactions on Industrial Electronics*, Vol. 56, NO. 5, May 2009.

[18] Y. I. Son, I. H. Kim, D. S. Choi, H. Shim, "Robust Cascade Control of Electric Motor Drives Using Dual Reduced-Order PI Observer," *IEEE Transactions on Industrial Electronics*, Early Access.

[19] Y. Tian, Z. Chen, F. Deng, X. Sun, Y. Hu, "Active Power and DC Voltage Coordinative Control for Cascaded DC-AC Converter with Bidirectional Power Application," *IEEE Transactions on Power Electronics,* Early Access.

[20] Goodwin G.C. Graebe, F.F, Salgado. M.E, Control system design, *[M] Upper Saddle River*, NJ : Prentice Hall, 2001.

[21] H. Qin, J. W. Kimball, "Generalized Average Modeling of Dual Active Bridge DC-DC Converter", *IEEE Transactions on Power Electronics*, Vol. 27, NO.4, 2012.

[22] R. W. A. A. De Doncker, D. M. Divan, M. H. Kheraluwala, "A three-phase soft-switched high-power-density DC/DC converter for high-power applications," *IEEE Transaction on Industrial Applications*, Vol.27, NO. 1, pp. 63-73, Jan/Feb. 1991.

[23] F. Krisme, J. W. Kolar, "Efficiency-Optimized High-Current Dual Active Bridge Converter for Automotive Applications," *IEEE Transactions on Power Electronics*, Vol. 59, NO. 7, July 2012.

[24] J. Shi, W. Gou, T. Zhao, A. Q. Huang, "Research on Voltage and Power Balance Control for Cascaded Modular Solid-State Transformer," *IEEE Transaction on Power Electronics*, Vol. 26, NO. 4, April 2011.

[25] L. Xue, Z. Shen, D. Boroyevich, P. Mattavelli, D. Diaz , "Dual Active Bridge-Based Battery Charger for Plug-in Hybrid Electric Vehicle with Charging Current Containing Low Frequency Ripple," IEEE Transactions on Power Electronics. IEEE Early Access Articles.

[26] J. Ge, Z. Zhao, L. Yuan, T. Lu, "Energy Feed-Forward and Direct Feed-Forward Control for Solid-State Transformer," *IEEE Transactions on Power Electroncis*, Early access.

[27] X. Sun, Y. Tian, Z. Chen, "Adaptive decoupled power control method for inverter connected DG," *I E T Renewable Power Generation* , Sep 2013.

[28] R. Teodorescu, M. Liserre, P. Rodr´iguez, "Grid Converters for Photovoltaic and Wind Power " pp 222.

[29] F. Liu, Y. Zhou, S. Duan, J. Yin, B. Liu, F. Liu, "Parameter design of a two-current-loop controller used in a grid-connected inverter system with LCL filter*," IEEE Transactions on Industrial Electronics*, Vol. 56, NO. 11, November 2009.

[30] H. Krishnamurthy, R. Ayyanar, "Stabitlity Analysis of Cascaded Converters for Bidirectional Power Flow Application", *Telecommunications Energy Conference*. San Diego, CA 14-18 Sept, 2008.

[31] K. Ogata, M. "Control Engineering", 5th Edition," in Prentice Hall, 2010 pp 225.

[32] R.D. Middlebrook, "Input filter considerations in design and application of switching regulators, " in *Proc. IEEE IAS*,1979, pp 366-382.

[33] J. Wang, D. Howe, "A Power Shaping Stabilizing Control Strategy for DC Power Systems With Constant Power Loads," *IEEE Transactions on Power Electronics*, Vol. 23, No. 6, November.

[34] A. Emadi, A. Khaligh, C. H. Rivetta, G. A. Williamson, "Constant Power Loads and Negative Impedance Instability in Automotive Systems: Definition, Modeling, Stability, and Control of Power Electronic Converters and Motor Drives," *IEEE Transactions on Vehicular Technology*, Vol. 55, No. 4, July 2006.

[35] Liutanakul P, Awan A.-B, Pierfederici, S. , Nahid-Mobarakeh, B. , Meibody-Tabar, F. "Linear Stabilization of a DC Bus Supplying a Constant Power Load: A General Design Approach," *IEEE Transactions on Power Electronics*, Vol. 25, NO. 2, Febrary 2010